Proceedings of the Indian National Science Academy (2026) 92:1080–1094
https://doi.org/10.1007/s43538-025-00468-1

RESEARCH PAPER

In-depth investigation of adsorption properties and non-covalent interaction analysis for molnupiravir drug (antiviral agent for SARS-CoV-2) on single-walled carbon nanotubes: a comprehensive D.F.T. analysis

Anoop Kumar Pandey[1] · Shashwat Shukla[1] · O. P. Yadav[1] · Vijay Singh[2] · Apoorva Dwivedi[3]

Received: 28 June 2024 / Accepted: 19 May 2025 / Published online: 6 June 2025
© Indian National Science Academy 2025

Abstract
Because of their potential for use in drug delivery and other therapeutic interventions, carbon nanotubes and drug interactions have attracted a lot of attention recently. Molnupiravir, an antiviral drug, has exhibited promising characteristics in the treatment of viral infections, including the COVID-19 virus. Understanding its adsorption behavior on SWCNTs is essential for optimizing drug delivery systems and enhancing drug efficacy. In this work, we have investigated the adsorption of Molnupiravir on SWCNTs using a strong Density Functional Theory (DFT) framework. DFT calculations offer an influential contrivance for understanding the electronic structure, bonding, and energy changes associated with this interaction. This study delves into a thorough examination of the adsorption behavior and the Gibbs free energy associated with the interaction of Molnupiravir drug with SWCNTs. Employing a comprehensive DFT methodology, this research provides a detailed exploration of the molecular-level interactions and their implications. Our analysis reveals the intricate details of the adsorption process. We explore the electronic structure of the drug-nanotube complex, shedding light on the nature of the intermolecular exchanges. Furthermore, we calculate the Gibbs free energy of the system, providing insights into the thermodynamic stability and feasibility of the adsorption process. This comprehensive study advances our understanding of the interaction between Molnupiravir and SWCNTs. The insights gained from this research can guide the scheme and growth of drug delivery schemes and nanotherapeutics. Ultimately, this work contributes to the broader field of nanomedicine and molecular modeling, offering potential avenues for the efficient delivery of antiviral drugs.

Keywords Molnupiravir · Single-walled carbon nanotubes · Adsorption · Density functional theory · Gibbs free energy · Drug delivery · Nanomedicine · Molecular modeling

Introduction

In December 2019, Wuhan, China became the epicenter of COVID-19, an infectious respiratory disease brought on by the SARS-CoV-2 virus. This resulted in a worldwide pandemic that had a significant effect on social systems, economies, and public health (Celik 2023; Jiménez-Alberto et al. 2020). An antiviral medication called molnupiravir was first created by Emory University and Ridgeback Biotherapeutics to treat this illness. These days, Merck & Company produces it, and Lagevrio is the brand name under which it is sold (Antiviral and for COVID-19 2021). This drug works by creating mistakes in the virus's genetic code, which prevents it from replicating and spreading. When taken orally, molnupiravir is effective against a variety of RNA viruses, including SARS-CoV-2 (Abdelnabi et al. 2021). The current work explores an in silico analysis of the physico-chemical properties of CNT-molnupiravir complex in light of these noteworthy advancements. We have utilized the widely used Density Functional Theory (DFT) method to accomplish this.

✉ Apoorva Dwivedi
apoorvahri@gmail.com

[1] Department of Physics, K. S. Saket P.G. College, Ayodhya, India

[2] University of Dodoma, Dodoma, Tanzania

[3] Department of Applied Science and Humanities, Seth Vishambhar Nath Institute of Engineering and Technology, Barabanki, India

In order to assess the drug's comparative reactivity, we have derived global reactivity descriptors through the energy calculations of the Highest and Lowest orbitals. Furthermore, our investigation incorporates molecular docking techniques to explore the interaction sites of molnupiravir with the protein receptor of covid virus (Tiwari et al. 2020, 2022a, b). In 1991, Sumio Iijima's groundbreaking discovery of carbon nanotubes (CNTs) marked the genesis of a transformative era in nanotechnology, reshaping industries and propelling innovation in the realm of nanotechnology (Lijima 1991). Carbon nanotubes, with their exceptional chemical and physical properties, present a vast canvas of opportunities, particularly in the domain of drug delivery. CNTs have emerged as capable candidates for in vitro and in vivo drug delivery, leveraging their exceptional ability to penetrate biological barriers without inducing apparent cytotoxicity in human cells. Their hollow, cylindrical structure allows for the encapsulation of small drug molecules within their internal cavities (Lamberti et al. 2015; Brhane and Gabriel 2016). In drug delivery systems, active pharmaceutical agents are intricately coupled with these versatile carriers. The remarkable surface area-to-volume ratio and cylindrical geometry of CNTs offer a heightened probability of interactions with drug compounds (Heister et al. 2012). Additionally, the extended surface area of CNTs can be skillfully tailored with hydrophilic or amphiphilic polymers, further enhancing their carrier capabilities. Through functionalization, CNTs exhibit inner-cavity tethering and surface adsorption, offering multifaceted avenues for transporting pharmaceutical agents (Liu et al. 2007a, b, c). These inherent advantages position CNTs as a promising and versatile drug delivery system with the potential to significantly advance therapeutic approaches (Arsawang et al. 2011; Chen et al. 2011; Dwivedi and Pandey 2014). Molnupiravir (MPV) has gained considerable attention in recent years due to the infection of severe acute respiratory syndrome coronavirus-2 (SARS-CoV-2). Since some people infected with COVID-19 experience fever and headaches, paracetamol (PCM) has been prescribed to relieve these symptoms. Therefore, there is an urgent need to monitor and detect these drugs simultaneously in pharmaceutical and biological samples. In this regard, we developed a novel sensor based on nanoceria-loaded MWCNTs (CeNPs@MWCNTs) for simultaneous monitoring of MPV and PCM (X-Yahya et al. 2024). In literature, Azam Iraji zad et al. have presented a work entitled "A step toward Molnupiravir, COVID-19 Antiviral, detection using Cauliflower-Like cobalt Sulfide-Decorated carbon nanotube modified glassy carbon electrodes" to developed & fabricate high-performance Molnupirvir sensing platforms through a facile and scalable approach. Accordingly, multi-walled carbon nanotubes (MWCNTs) are first drop-casted on the surface of glassy carbon electrode. Afterward, cauliflower-like cobalt sulfide nanosheets are electrodeposited onto the MWCNT-casted electrode. The Molnupirvir-sensing ability of the prepared sensing platforms is evaluated using various electrochemical methods (Y- Elham Khezerloo 2024).

Using CNTs for drug delivery faces challenges like toxicity, poor solubility, and difficulty in targeted drug elimination, but these can be mitigated through surface functionalization and careful design.

In our current research endeavors (Misra et al. 2012; Dwivedi and Kumar 2019; Apoorva Dwivedi et al. 2024; Dwivedi et al. 2024), we have engaged in an exploration of the relative structural stability in the adsorption of molnupiravir by CNT (C56H16). Our investigation extends to the examination of the chemical properties inherent to the CNT-molnupiravir complex, employing a comprehensive analysis involving electronic plots, using the DFT/6-31G (d, p) methodology. Furthermore, we have delved into the NBO and AIM studies of the CNT-molnupiravir system. This research effort serves to unveil significant interaction sites, shedding light on diverse pathways of drug absorption. It contributes valuable insights into the various mechanisms underlying the adsorption of drugs in this context.

Computational details

The examination of molnupiravir absorption by carbon nanotubes (CNT) takes place in a dimethyl sulfoxide (DMSO) solvent environment. To optimize the various potential interactions of molnupiravir, we utilize the HF/3-21G method, free from symmetry constraints. Subsequently, the lowest energy conformer is further optimized through DFT/B3LYP technique and the 6-31G (d, p) basis set (Becke 1993a; Lee et al. 1988), using the Gaussian 09 W package (Frisch et al. 2003). The geometries of both CNT and molnupiravir are subjected to optimization at the same level of theory. Our analysis extends to AIM (Atoms in Molecules) assessments for the CNT-molnupiravir complex. We delve into a comprehensive exploration of electronic properties by generating HOMO, LUMO, and MESP plots, with the assistance of Gauss-View (Frisch et al. 2000), a widely-used graphical user interface for Gaussian software. For UV spectra analysis, TDDFT is employed to plot the UV spectra of CNT and the CNT-molnupiravir complex, adopting the same theoretical level in a water-based solvent. Other electronic parameters are meticulously calculated based on the optimized structures of CNT, CNT-molnupiravir, and molnupiravir. The Polarized Continuum Model (P.C.M.) is harnessed to incorporate solvent effects and generate the Density of States (DOS) plot (O'Boyle et al. 2008) for both CNT and CNT-molnupiravir. Furthermore, the IEFPCM model is applied to compute proton NMR chemical shifts, offering a comprehensive understanding of the electronic and spectroscopic properties in this intriguing system.

Results and discussion

Geometry optimization

We conducted an extensive study to investigate the interactions between a carbon nano tube (CNT) with the chemical compound molnupiravir (C56H16). We employed the Hartee Fock technique to model various possible configurations and optimize their geometries. Geometries of CNT (C56H16) and Molnupiravir are presented in Fig. 1. In Fig. 2, we present the Most stable optimized Geometry of CNT (C56H16)@Molnupiravir. This identified lowest energy structure displays stable characteristics as all of its vibrational frequencies are positive. In Fig. 2, the interaction between CNT and molnupiravir involves specific interactions with nearby hydrogen atoms of the CNT. Notably, both structures are oriented perpendicularly to each other. To gain a more detailed understanding, we further optimized the lowest energy conformer (CNT) and molnupiravir using the DFT/B3LYP method in conjunction with the 6-31G (d, p) basis set. The results of this optimization, including the structural parameters of the CNT-molnupiravir interaction, are summarized in Table 1. An intriguing finding is that the bond lengths of molnupiravir are significantly altered upon absorption by the CNT, particularly at the sites where non-bonded interactions occur. Specifically, the N–H bond length of molnupiravir increases by 0.02 Å (angstrom) in one dimension and 0.001 Å in another, while the C–C bond length decreases by 0.02 Å. Additionally, the C–C bond length of the CNT experiences a slight increase after absorbing molnupiravir. However, the C–H bond length exhibits a reverse effect. The majority of other bond lengths within the CNT remain largely unaffected following the absorption of molnupiravir. The observed changes in bond lengths within the CNT after the absorption of molnupiravir introduce polarity and give rise to non-bonding and hydrogen-bonding interactions. To gain further insights into these variations in charge density and interaction strength, we conducted an AIM (Atoms in Molecules) analysis of the CNT after the absorption of molnupiravir. This analysis allows us to investigate the nature of these interactions in more detail.

QTAIM analysis

In the context of the Quantum Theory of Atoms in Molecules (QTAIM), electron density values provide insights into the nature and strength of chemical bonds, revealing information about atomic interactions and charge distribution within molecules. QTAIM identifies "bond paths" between atoms, and the point on these paths with the lowest electron density is the BCP. The electron density value at the BCP is a key indicator of bond strength and type. The Laplacian ($\nabla^2\rho$) of the electron density indicates charge concentration or depletion. A negative Laplacian

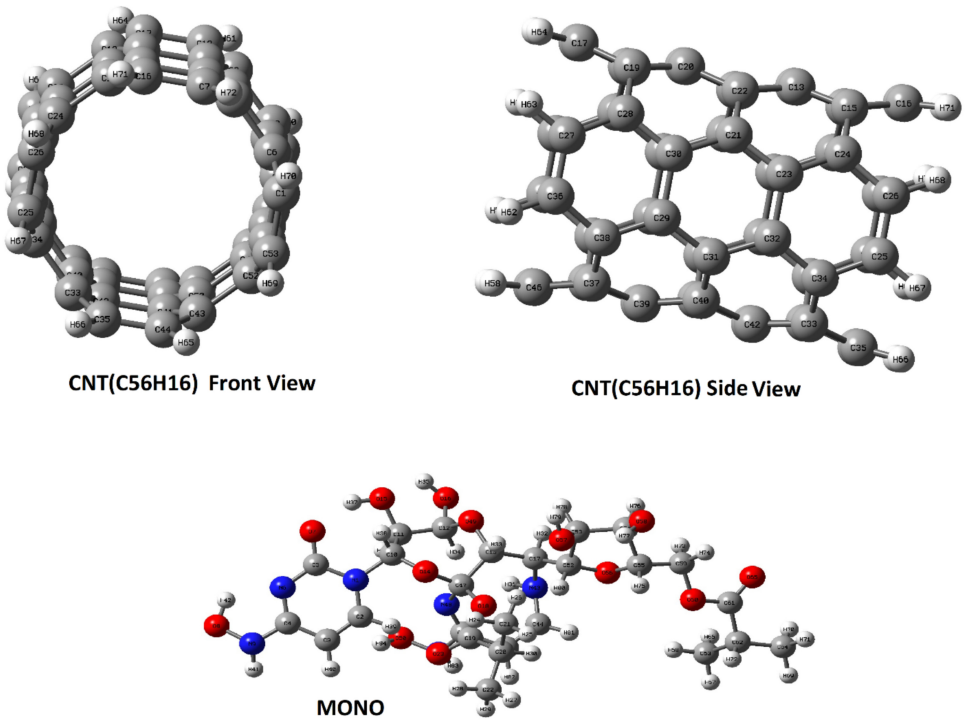


Fig. 1 Geometries of CNT (C56H16) and molnupiravir

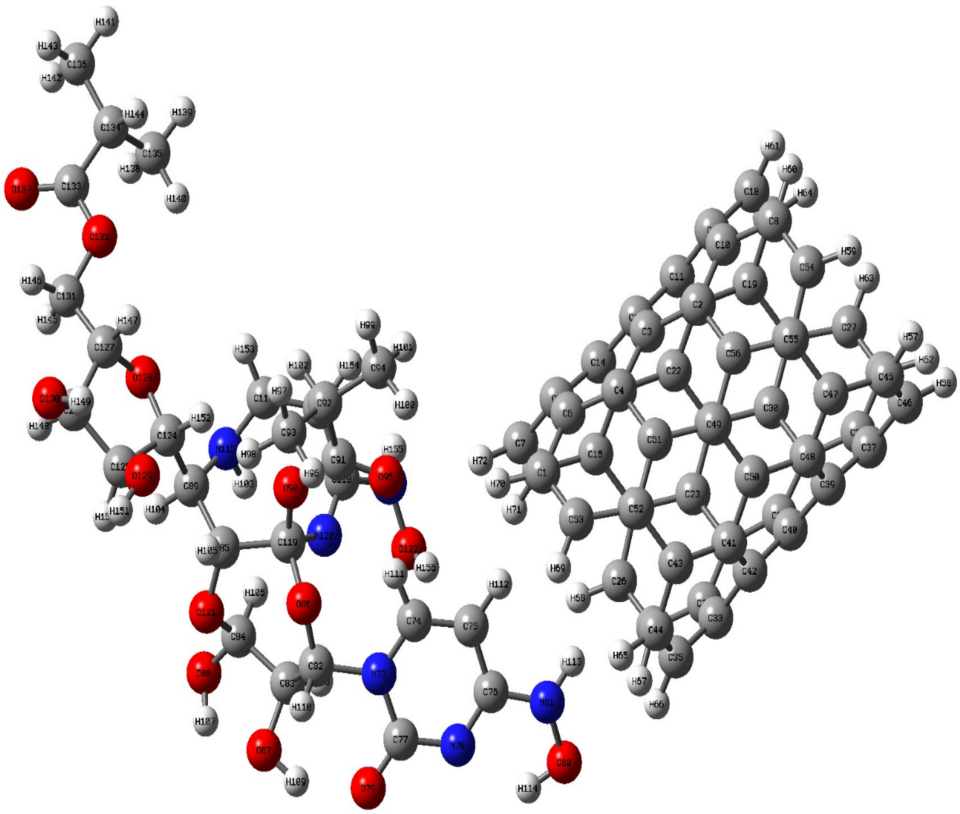


Fig. 2 Most stable optimized geometry of CNT (C56H16) @ molnupiravir

value suggests a local concentration of charge, while a positive value indicates depletion. QTAIM can also analyze intermolecular interactions, such as hydrogen bonds, by examining the electron density and it's Laplacian in the region between interacting atoms. QTAIM allows for the calculation of atomic charges by integrating the electron density over the atomic basins, providing a more rigorous definition of atomic charges compared to other methods. QTAIM is used in various fields, including materials science, drug discovery, and catalysis, to study chemical bonding, reactivity, and other properties of molecules and materials (Matta and Boyd 2007).

Using certain topological parameters at the Bond critical point (BCP), the quantum theory in atoms is a useful tool to determine nonbonding interaction in atoms (Matta and Boyd 2007). Nonbonding criteria (Bader 1991) state that the Laplacian (Δ^2ρbcp) and electron density (ρbcp) should lie between 0.024 and 0.139 au and 0.002 and 0.040 au, respectively. There are eight nonbonding interactions in CNT@ molnupiravir. Table 2 lists a number of topological parameters, such as charge density ($\boldsymbol{\rho_{bcp}}$) Laplacian electron density [∇^2 ρ(r)] potential energy (V_{BCP}), kinetic energy density (G_{BCP}), and total energy density (H_{BCP}) at BCP. Figure 3 displays the title molecule's nonbonding interaction molecular graph. Laplacian ∇^2 ρ(r) resolves the structure of any chemical system (Koch and Popelier 1995). Laplacian increases are therefore directly proportional to the bond lengths of both associated atoms, as indicated by the calculated value of ∇^2 ρ(r) > o, which indicates that ρ(r) is connected with bond length between both associated atoms.

Closed shell H-bonding is indicated by the highest value of Δ2ρbcp = The calculated ρ(r) falls in 10–2 for H111-O86. The remaining seven interactions, denoted by ρ(r), lie within the range of 10–3, meaning that all six nonbonding interactions are part of the Vander Wall interactions (Cremer and Kraka 1984). The total energy at BCP, expressed as H(r) = V(r) + G(r), is both sign and magnitude (Bader 1990; Bader and Esse´n 1984). When V(r) has a negative sign and G(r) is always positive, it can be inferred that G(r) > V(r) indicates that one connected atom has more electron density shifted than the other; conversely, when H(r) < 0, it can be inferred that V(r) > G(r) indicates that both atoms share electron density. The explanation above demonstrates that determines the nature of chemical bonding. For all nonbonding interactions, this means that V(r) < G(r), implying that all interactions are of an ionic nature. Rozas et al. (2000) have confirmed this, using the criteria ∇2ρbcp > 0 and H > 0. The primary curvatures of a bond at the BCP of the Laplacian ∇2ρ(r) are the. Another index is also highly helpful in identifying the type of chemical bonding (Rozas et al. 2000). All eight interactions are shown to be closed shell interactions by the current computation. The following equation, ΔEint = 1/2 (VBCP), is used to

Table 1 Range of optimized equilibrium parameters of molnupiravir, CNT, and CNT-molnupiravir

Molecule	Parameter	B3LYP/6–31 (d, p)
Molnupiravir	C=N	1.28 = 1.37
	N–O	1.39
	C–O	1.35–1.42
	C–N	1.41–1.46
	(C=C) aro	1.36–1.42
	C=O	1.21–1.23
	(C–C) non-aro	1.50–1.57
	(C–H) ring	1.076–1.081
	C–H	1.081–1.087
	N–H	1.011–1.012
	O–H	0.968–0.986
CNT (C56-H16)	C–C	1.372–1.448
	C=C	1.372–1.448
	C–H	1.086
CNT- Molnupiravir	C=N	1.29 = 1.39
	N–O	1.39
	C–O	1.35–1.42
	C–N	1.39–1.46
	(C=C) aro	1.36–1.42
	C=O	1.21–1.23
	(C–C) non-aro	1.52–1.56
	(C–H) ring	1.077–1.081
	C–H	1.014–1.087
	N–H	1.011–1.03
	O–H	0.975–0.986

calculate the strength of interactions. H111-O86 exhibits weak interactions (5 > Eint > 12 kcal/mol); on the other hand, O122-H71, N81-H86, C74-H156, and O84-H63 exhibit very weak interactions (Eint > 1 kcal/mol). Vander Waals' interaction includes Eint < 1 among the remaining four interactions (Espinosa et al. 1998).

Thermodynamic stability

In this section, we assessed the thermodynamic stability of CNT@molnupiravir, achieved through the absorption of molnupiravir by a carbon nanotube (CNT) with a chemical formula of C56H16. To determine the absorption energy of CNT@molnupiravir, we utilized the following calculation:

$$\text{Adsorption energy (Ead)} = [\text{ECNT(C56H16)} - \text{molnupiravir} - \{\text{E molnupiravir} + \text{ECNT(C56H16)}\}] \quad (1)$$

where the electronic energies of suffices are represented by ECNT(C56H16)-molnupiravir, E molnupiravir, and ECNT(C56H16). Table 3 lists the estimated Gibbs free energy (G), enthalpy (H), and entropy (S) of the reaction, CNT, molnupiravir, and CNT@ molnupiravir at 25 °C. The Gibbs free energy of CNT@molnupiravir, we employed the following calculation:

$$\text{Gibbs Free energy}(\Delta G) = \left[(\Delta G)\text{CNT(C56H16)} - \text{molnupiravir} - \{(\Delta G)\text{molnupiravir} + (\Delta G)\text{CNT(C56H16)}\}\right] \quad (2)$$

At room temperature 300 K, the adsorption of molnupiravir with CNT favored forward direction, as indicated by the calculated absorption energy [$\Delta\varepsilon ad > 0$]. The enthalpy (ΔH), entropy (ΔS), and Gibbs free energy (ΔG) for the CNT adsorption reaction all change negatively. It indicates that although the reaction is exothermic, it proceeds forward and does so spontaneously. The equilibrium constant (keq), which is associated with the Gibbs free energy (ΔG), and the residual thermal energy (RT) are related thermodynamically by.

$$\text{Keq}\alpha \exp\left(\frac{-\Delta G}{RT}\right) \quad (3)$$

The calculated value equilibrium constant ($K_{eq} = 49.95$) at room temperature shows reaction proceed forward direction

Table 2 Calculated topological parameters $\rho_{bcp\ (au)}$ $\nabla^2\rho_{bcp}$ (au), $\left[\frac{\lambda_1}{\lambda_3}\right]$, G_{Bcp} (au), V_{Bcp} (au) Eint (kcal/mol) at BCP of CNT@ molnupiravir

Bond	ρ_{bcp}	$\nabla^2\rho_{bcp}$	Ratio of Eigen value $\nabla^2\rho_{bcp}$ $\left[\frac{\lambda_1}{\lambda_3}\right]$	G_{BCP}	V_{BCP}	$\left[\frac{V(r)}{G(r)}\right]$	H_{BCP}	E_{int} (kcal/mol)
O_{122}–H_{71}	0.00573	0.00313	0.142759	0.00558	−0.00333	0.596774	0.00225	1.04479
O_{95}–H_{70}	0.00367	0.02187	0.138318	0.00360	−0.00173	0.480556	0.00187	0.54279
O_{95}–H_{72}	0.00196	0.01215	0.123919	0.00189	−0.00074	0.391534	0.00115	0.23218
O_{86}–H_{111}	0.01995	0.09795	0.172995	0.02183	−0.01917	0.878149	0.00266	6.01459
C_1–H_{112}	0.00548	0.02163	0.160864	0.00409	−0.00278	0.679707	0.00131	0.87223
N_{81}–H_{86}	0.00721	0.03115	0.141768	0.00610	−0.00442	0.72459	0.00168	1.38678
N_{120}–H_{111}	0.01286	0.05118	0.150807	0.00399	−0.00268	0.671679	0.00131	0.84085
C_{74}–H_{156}	0.00925	0.03388	0.205132	0.00697	−0.00546	0.783357	0.00151	1.71308

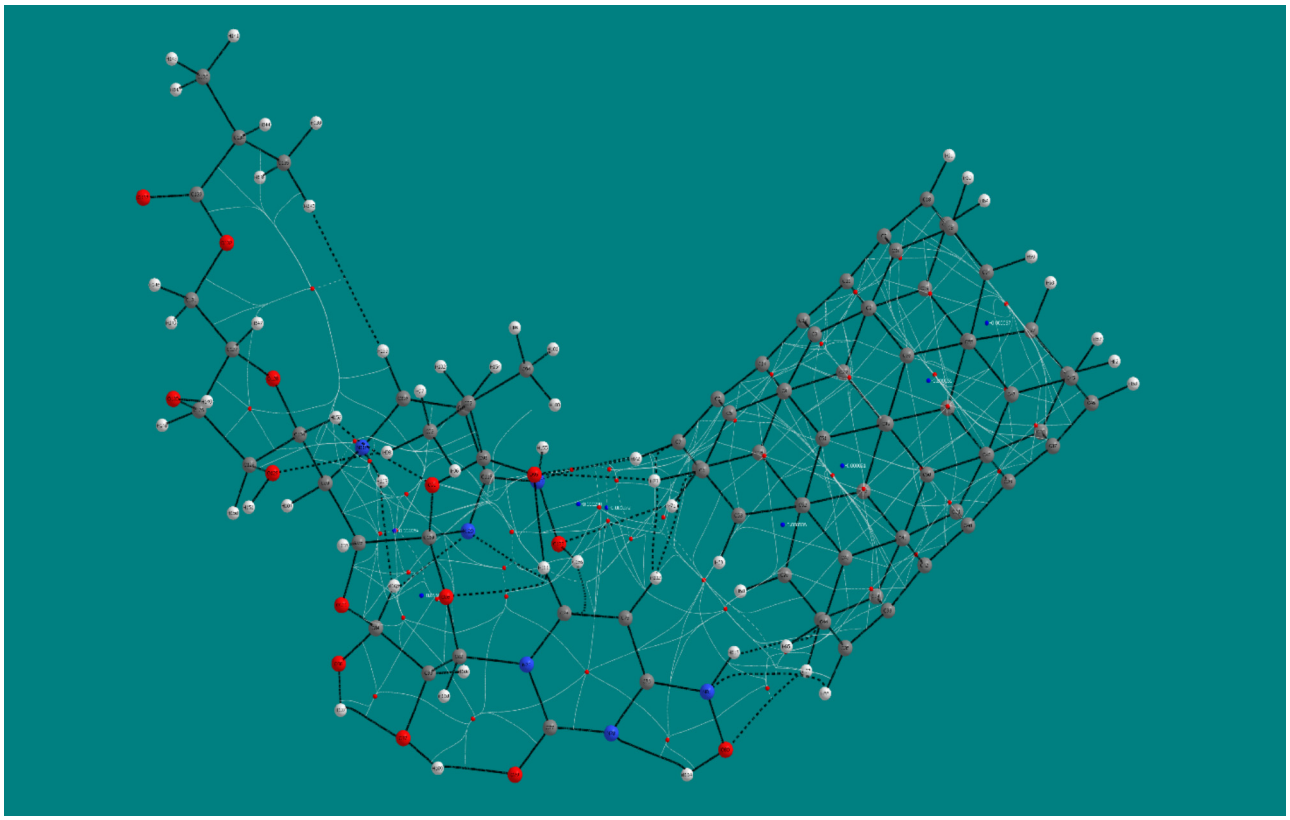


Fig. 3 Molecular graph of QTAIM analysis of CNT@ molnupiravir

Table 3 Calculated thermodynamical parameters for formation of CNT@ molnupiravir

Species	Electronic (au)	Enthalpy (au)	Gibbs Free energy(au)	Entropy (kcal/mol-K)	K_{eq} of Reaction
CNT56	−2141.71	−2141.69	−2141.76	164.302	–
Molnupiravir	−2393.4	−2393.35	−2393.48	268.578	–
CNT@ molnupiravir O	−4535.12	−4535.05	−4535.23	390.893	–
CNT + molnupiravir → CNT@ molnupiravir	−0.01338	−0.0132	0.00769	−41.987	49.9499

at room temperature which confirm adsorption of molnupiravir with CNT.

Electronic properties

Frontier molecular orbitals define the nature and chemical reactivity of molecules. Frontier molecular orbitals are HOMO and LUMO. The energy gap is the amount of energy needed for an electron to move from a HOMO to a LUMO. Less chemical reactivity or greater kinetic stability result from the higher transition energy, this indicates that more energy is needed for the electron transition from HOMO to LUMO. Chemical reactivity is inversely correlated with the energy gap (Fleming 1976; Murray and Sen 1996). While LUMO primarily serves as an acceptor, HOMO primarily serves as a donor. Figure 4 displays the HOMO and LUMO plot of CNT@ molnupiravir. Both the HOMO and LUMO are dispersed close to the CNT region. A sigma bond's (σ) lowest unoccupied molecular orbital (LUMO) can be excited by electrons occupying its HOMO (highest occupied molecular orbital). The transition $\sigma \rightarrow \sigma^*$ is used to represent this process.

For CNT56, CNT@ molnupiravir, and molnupiravir, which are listed in Table 4, the global electronic descriptors such as band gap electronegativity, chemical potential, chemical hardness, chemical softness, and global electrophilicity index are also calculated. The band gap between HOMO and LUMO as well as chemical stability are related to the chemical hardness

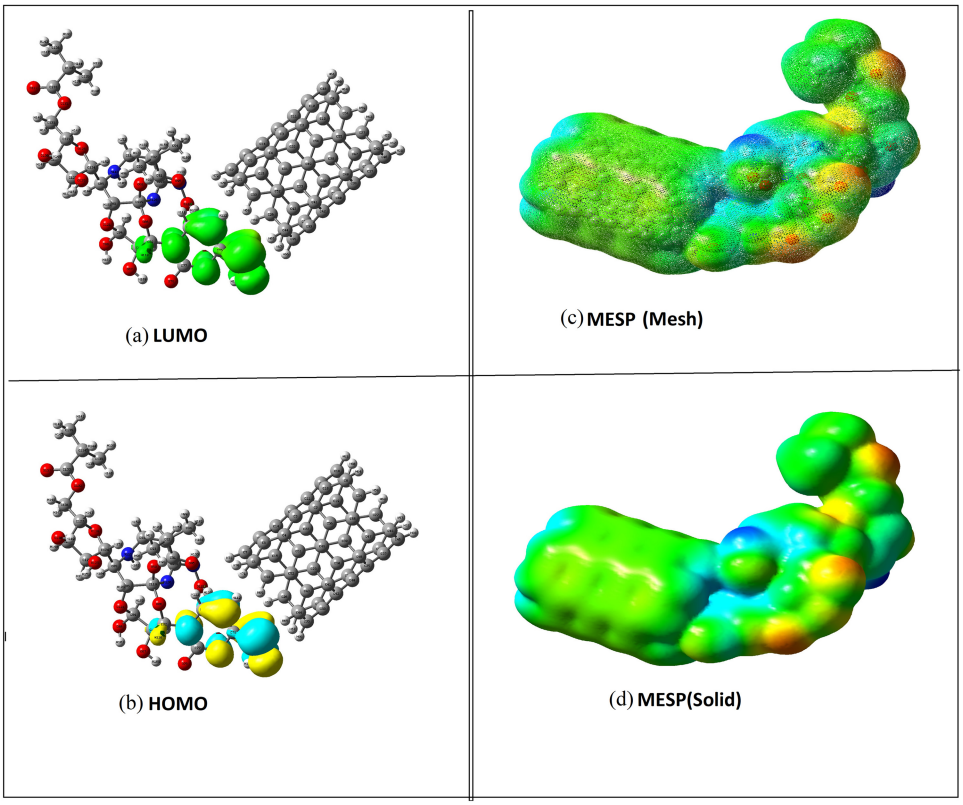


Fig. 4 **a** LUMO, **b** HOMO and MESP plots [**c** MESP-Mesh and **d** of CNT (C56H16)@ molnupirvir]

Table 4 The EHOMO, ELUMO, Energy gap (E_L–E_H), Chemical Potential (μ), Electronegativity (χ), Global Hardness (*η*), Global Softness (S) and Global Electrophilicity Index (ω) of Molnupiravir, CNT@ Molnupiravir and CNT

Property	Molnupiravir	CNT	CNT@ molnupiravir
Dipole moment (μ) (D)	10.459	0.0	8.730
E_{HOMO}(eV)	−7.66607	−4.463	−5.48323
E_{LOMO}(eV)	−0.18585	−2.476	−1.53278
E_{GAP} (eV)	7.480221	1.986	3.950449
χ(eV)	3.92596	3.469	3.508003
μ(eV)	−3.92596	−3.469	−3.50800
$\eta(eV)^{-1}$	3.740111	0.993	1.975225
S(eV)	0.133686	0.504	0.253136
ω(eV)	2.060522	6.059	3.115111
ΔN_{max}	1.049691	3.493	1.776002

value. The energy differential between LUMO and HOMO is equivalent to the chemical hardness. The system's ionization potential and electronegativity are equivalent to the negative values of the LUMO and HOMO eigenvalues, respectively.

$$\text{Energy band gap} = (\varepsilon\text{LUMO} - \varepsilon\text{HOMO}) \quad (4)$$

$$\text{Electronegativity}\,(\chi) = 1/2(\varepsilon\text{LUMO} + \varepsilon\text{HOMO}) \quad (5)$$

$$\text{Chemical potential}\ \mu = -\chi \quad (6)$$

$$\text{Global hardness}\ \eta = {}^{1}/_{2}(\varepsilon\text{LUMO} - \varepsilon\text{HOMO}) \quad (7)$$

$$\text{Global softness}\ (S = 1/2\eta) \quad (8)$$

$$\text{Global electrophilicity index}\omega = \mu 2/2\eta \quad (9)$$

Chemical Hardness (η) is a measure of a molecule's resistance to deformation of its electron density, indicating its stability while Chemical Softness (S) is the inverse of hardness, reflecting a molecule's tendency to polarize or undergo electron transfer. Electrophilicity (ω) is a measure of a molecule's tendency to attract electrons, indicating its electrophilic character while Electronegativity (χ) is a measure of an atom's ability to attract electrons in a chemical bond.

Chemical Potential (μ) is a measure of the average electron energy in a molecule (Parr and Pearson 1983; Geerlings et al. 2003; Parr et al. 1999; Ayers and Parr 2000; Erdogdu et al. 2010).

From the table, this can easily be interpreted that the global electronic descriptor of CNT changes after absorption of molnupiravir. The chemical hardness (η) of CNT decrease after absorption of molnupiravir while electrophilicity index (ω) of CNT decrease after absorption of

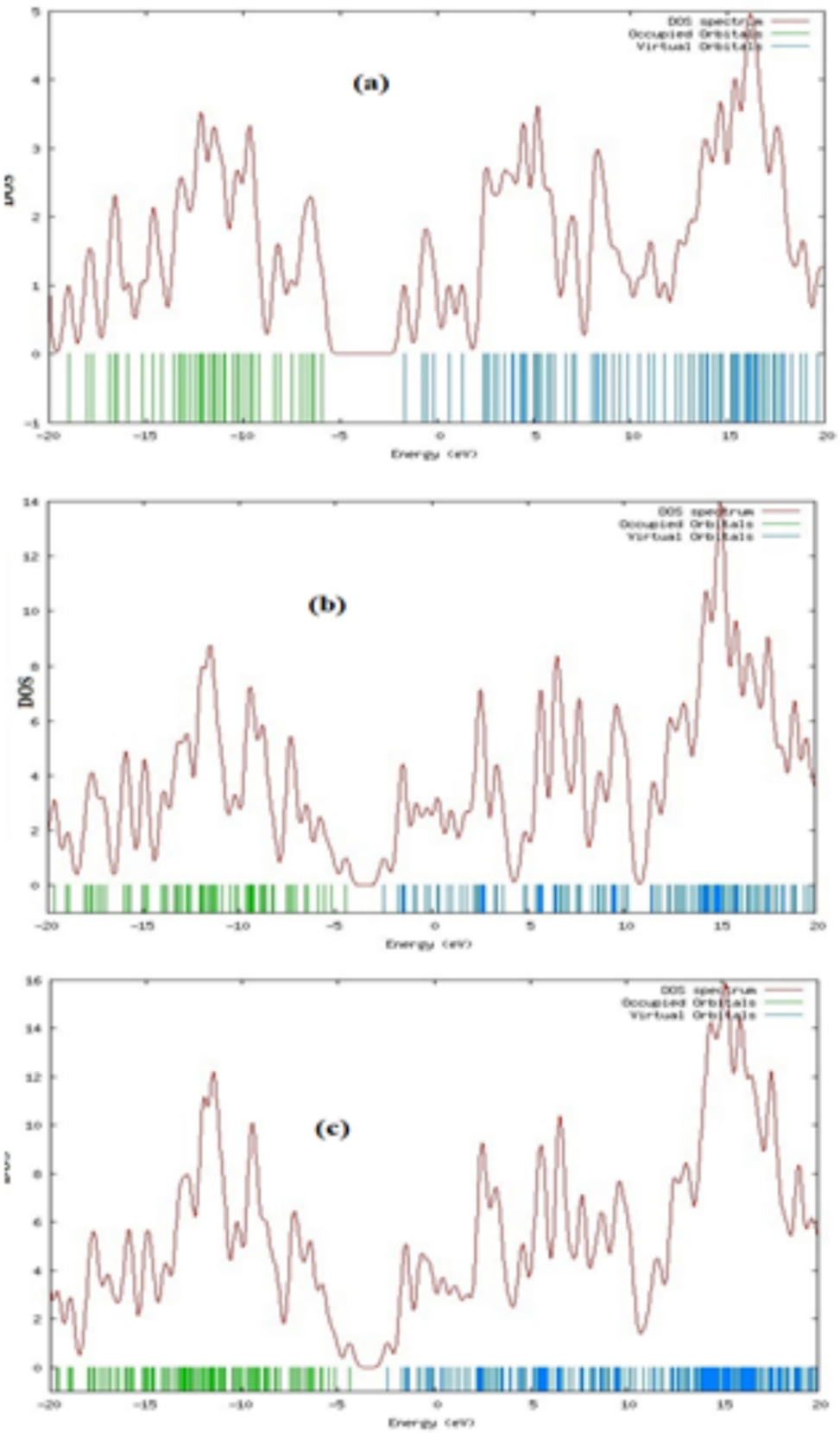


Fig. 5 Comparison of density of state spectra of **a** Molnupiravir, **b** CNT and **c** Molnupiravir @ CNT

Table 5 TDDFT calculation of CNT@ molnupiravir in water solvent by using B3LYP/6-31G (d)

S. N	Transition	Wave length (nm) λ_{max}	Transition energy (eV)	Oscillatory strength	Orbitals transition % contri
1	$S_0 \rightarrow S6$	387	3.2069	0.0018	H → L + 5 (93%)
2	$S_0 \rightarrow S_7$	378	3.2823	0.0588	H-1 → L(50%), H → L + 1 (−49%)
3	$S_0 \rightarrow S_{14}$	334	3.7141	0.0055	H-1 → L + 2 (−12%), H-1 → L + 3 (−11%), H → L + 9 (50%
4	$S_0 \rightarrow S_{15}$	333	3.7251	0.0085	H-1 → L + 4 (20%), H → L + 10 (51%)H-7 → L (7%)
5	$S_0 \rightarrow S_{16}$	316	3.9277	0.0123	H-1 → L + 4 (14%), H → L + 10 (18%), H → L + 11 (17%
6	$S_0 \rightarrow S_{17}$	315	3.9354	0.0296	H-1 → L + 2 (12%), H → L + 9 (20%), H → L + 12 (−13%)H-12 → L (5%)
7	$S_0 \rightarrow S_{19}$	303	4.0890	0.0470	H-7 → L (15%), H-2 → L + 2 (20%), H-2 → L + 3 (11%), H-1 → L + 4 (13%)
8	$S_0 \rightarrow S_{20}$	302	4.1019	0.0446	H-8 → L (10%), H-2 → L + 4 (36%)
9	$S_0 \rightarrow S_{23}$	289	4.2892	0.2725	H-8 → L (38%), H-2 → L + 1 (12%), H-1 → L + 2 (−33%)
10	$S_0 \rightarrow S_{24}$	288	4.2938	0.0798	H-2 → L + 1 (49%), H-1 → L + 3 (34%)H-8 → L (8%),
11	$S_0 \rightarrow S_{25}$	287	4.3005	0.3830	H-7 → L (41%), H-1 → L + 4 (40%)
12	$S_0 \rightarrow S_{27}$	277	4.4709	0.0036	H-3 → L + 5 (14%), H-1 → L + 9 (16%), H → L + 6 (35%), H → L + 7 (16%)
13	$S_0 \rightarrow S_{28}$	278	4.4792	0.0022	H-4 → L + 5 (17%), H-3 → L + 5 (12%), H-1 → L + 10 (33%)
14	$S_0 \rightarrow S_{30}$	272	4.5577	0.2682	H-4 → L + 1 (12%), H-3 → L + 1 (57%)

Table 6 TDDFT calculation of molnupiravir in water solvent by using B3LYP/6-31 G (d)

S. N	Transition	Wave length (nm) λ_{max}	Transition energy (eV)	Oscillatory strength	Orbitals transition % contri
1	$S_0 \rightarrow S1$	267	4.6459	0.1423	H → L (55%), H → L + 1 (37%)
	$S_0 \rightarrow S2$	244	5.0818	0.3516	H-1 → L (40%), H-1 → L + 1 (38%)
2	$S_0 \rightarrow S3$	235	5.2819	0.3516	H-6 → LUMO (10%), H-5 → L (15%), H-5 → L + 1 (11%), H-2 → L (26%), H-2 → L + 1 (15%)
	$S_0 \rightarrow S4$	218	5.7013	0.1565	H-3 → L(20%), H-3 → L + 1 (28%), H-2 → L (11%)
3	$S_0 \rightarrow S5$	217	5.7013	0.0156	H-3 → L(13%) + H-3 → L + 1 (9%), H-2 → L(9%), H-2 → L + 1 (9%)
4	$S_0 \rightarrow S9$	202	6.1436	0.1024	H-1 → L + 2 (34%), H-1 → L + 3 (24%)
5	$S_0 \rightarrow S_{14}$	192	6.4561	0.0353	H-2 → L + 1 (10%), HOMO → L + 2 (−10%), HOMO → L + 3 (21%), HOMO → L + 5 (16%)
6	$S_0 \rightarrow S_{15}$	189	6.6340	0.0536	H-5 → L (10%), H → L + 3 (10%)
7	$S_0 \rightarrow S_{17}$	181	6.8320	0.0253	H-11 → L (10%), H-6 → L + 1 (26%), H- → 5- (−12%)
8	$S_0 \rightarrow S18$	189	6.8637	0.2402	H-3 → L + 2 (46%), H-3 → L + 3 (30%)
9	$S_0 \rightarrow S19$	188	6.9176	0.0517	H-7 → L (19%), H-4 → L (12%), H → L + 5 (20%)
10	$S_0 \rightarrow S_{21}$	177	6.9872	0.0303	H-4 → L (21%), H-4 → L + 1 (15%), H → L + 5 (23%)
11	$S_0 \rightarrow S_{27}$	169	7.3382	0.0136	H-3 → L (17%), H-3 → L + 1 (17%), H-1 → L + 3 (14%)
12	$S_0 \rightarrow S_{28}$	168	7.3475	0.0130	H-3 → LUMO (17%), H-3 → L + 1 (15%), H-1 → L + 2 (14%), H-1 → L + 3 (16%)
13	$S_0 \rightarrow S_{28}$	167	7.3729	0.0408	H-2 → L + 2 (10%), H-2 → L + 5 (16%)H-5 → L + 2 (5%), H-5 → L + 3 (−9%)
14	$S_0 \rightarrow S_{30}$	166	7.3930	0.0138	H-1 → L + 3 (12%), H-1 → L + 11 (16%)

molnupiravir. E_{gap} decreases while chemical softness(S) shows reverse effect after absorption of molnupiravir. The CNT gets polarized after the absorption of molnupiravir by CNT, hence the chemical stability of CNT decreases as compared with isolated molnupiravir. This fact can be further verified by the dipole moment of CNT (0 D), CNT- molnupiravir (8.730 D), and molnupiravir (10.459 D). The charge transfer between CNT and molnupiravir is the cause of the notable change in the dipole moment of CNT following molnupiravir absorption. The difference between the molnupiravir and carbon nanotube (CNT) interacting molecules' Δ Nmax as they approach one another defines the Electrophonic Charge Transfer (ECT), which is the process by which molnupiravir is absorbed by CNT (Padmanabhan et al. 2007). One way to determine the ECT value is by

Table 7 TDDFT calculation of CNT in water solvent by using B3LYP/6-31 G (d)

Excited state	E(eV)	Oscillatory strength (f)	Calculated (λmax)	Transition orbital's
$S_0 \rightarrow S_8$	2.597	0.5776	477	H-1 → L(51%), H → L + 1 (46%)
$S_0 \rightarrow S_{17}$	3.224	0.0343	384	H-6 → L(15%),H-1 → L + 3 (62%), H → L + 8 (15%)
$S_0 \rightarrow S_{23}$	3.477	0.0205	357	H-6 → L(10%), H-5 → L(30%), H-3 → L + 1 (31%)
$S_0 \rightarrow S_{24}$	3.478	0.0206	356	H-6 → L(30%),H-5 → L (-10%), H-4 → L + 1 (31%)
$S_0 \rightarrow S_{33}$	3.790	0.3822	327	H-5 → L(15%),H-4 → L + 1(20%),H-3 → L + 1(12%), H → L + 9 (20%)
$S_0 \rightarrow S_{34}$	3.790	0.3819	327	H-6 → L(15%),H-4 → L + 1(12%),H-3 → L + 1(20%), H → L + 10 (20%)

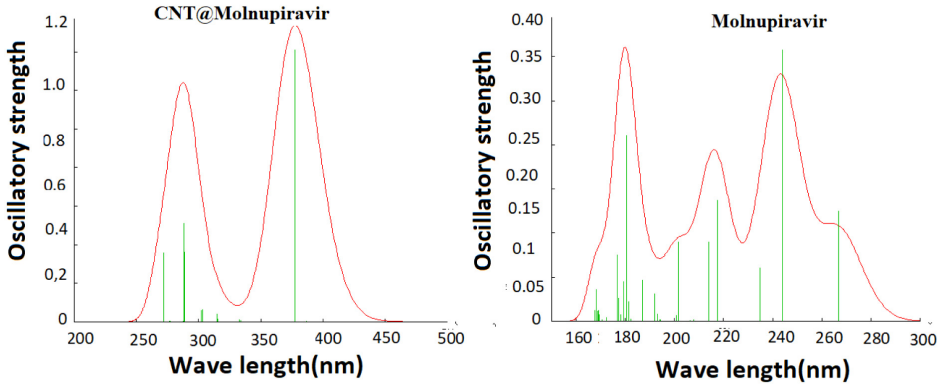


Fig. 6 Comparison of UV–Vis spectra of molnupirvir and CNT@molnupirvir

$$\mathrm{ECT} = (\Delta\mathrm{Nmax})\mathrm{CNT56} - (\Delta\mathrm{Nmax})\ \mathrm{molnupiravir} \tag{10}$$

$$(\Delta\mathrm{Nmax})\mathrm{CNT56} = -\frac{\mu_{\mathrm{CNT56}}}{\eta_{\mathrm{CNT56}}} \tag{11}$$

$$(\Delta\mathrm{Nmax})\ \mathrm{molnupiravir} = -\frac{\mu_{\mathrm{molnupiravir}}}{\eta_{4\mathrm{molnupiravir}}} \tag{12}$$

From our calculations, ECT (for molnupiravir and CNT) is 2.4434 > 0, meaning that the charge in the process of absorption of molnupiravir by CNT by CNT transfers from molnupiravir to CNT. This clearly shows that molnupiravir is electron efficient entity and behaves as a donor, however, CNT shows electron deficiency an; however as an acceptor. With a low electrophilicity index value and a high chemical potential, the CNT exhibits nucleophilic behavior.

Molecular electrostatic potential (MEP) analysis

Molecular electrostatic potential, or MEP, describes the electron density of any molecular system and offers important details about electrophonic and nucleophilic attacks. The relationship between MEP's physiochemical properties and molecular structure is defined (Becke 1993b; Bohl et al. 1984). MEP establishes a relationship between the chemical reactivity dipole moment, partial charges, and chemical reactivity site. Different colors indicate a molecule's strength of electrostatic potential. For example, red denotes a negative electrostatic potential, blue denotes the highest positive potential, and green denotes zero potential. Blue, green, yellow, orange, and red all have decreasing electrostatic potentials (Lewis and Griffiths 1987). Figure 4 displays the MEP plot of CNT-molnupiravir. Red surrounds the nitrogen (blue) of the CNT-molnupiravir ring, but yellow surrounds the CNT, making the CNT by itself electrically neutral (Fig. 5).

UV spectra

In our investigation, we delved into the flora of electronic shifts and UV spectra by employing Time dependent DFT scheme. We applied this level of theory to molnupiravir, CNT, and the interaction of molnupiravir with CNT. Using the IEFPMC model, these calculations were performed on the optimized molecular geometries in the presence of a water solvent. The outcomes of our TDDFT calculations include the determination of transition energies corresponding to absorption wavelengths, oscillatory strength, and the identification of transition orbitals for both CNT-molnupiravir and CNT. The relevant data are presented in Tables 5,

Table 8 Calculated NMR parameters (CSA) and (CSI) in ppm for CNT@ molnupiravir, molnupiravir, and CNT of interacting atoms

S.N	Atoms	Gas	
		Chemical shift anisotropic (CSA.)	Chemical shift isotropic (CSI.)
CNT@ Molnupiravir			
1	C75	100.8039	109.1368
2	C76	144.1047	34.2823
3	C36	157.7595	72.7641
4	C19	168.8084	74.2160
5	C17	157.4653	72.8339
6	N81	100.6755	57.8244
7	O80	234.5980	111.7657
8	O122	78.2990	224.4775
9	O95	558.8164	55.1774
10	H114	14.6232	24.0473
11	H112	6.4685	24.0127
12	H113	7.2116	22.8838
13	H154	4.8722	27.0770
14	H65	5.6113	22.8023
15	H66	5.2790	22.6228
16	H70	3.5886	22.4442
17	H67	5.5206	22.7351
18	H68	4.9942	23.0786
19	H69	7.4114	24.6806
Molnupiravir			
1	N9	65.1308	117.3489
2	N6	269.6505	64.1746
3	O8	108.3519	228.1472
4	O7	414.4349	34.2956
5	O15	43.4146	280.1684
6	C5	79.3059	43.3704
7	C22	22.1380	175.2738
8	H41	6.4658	26.5947
9	H42	14.1646	14.1646
10	H37	24.4564	25.9610
11	H35	26.5947	27.6005
CNT56			
1	C36	152.29	71.60
2	C37	160.68	74.00
3	C38	160.66	74.03
5	C27	152.22	71.62
6	C46	152.25	71.63
7	H62	6.20	22.95
8	H63	6.20	22.95
9	H58	6.18	22.95

6 & 7. Moreover, the calculated UV spectra for CNT-molnupiravir and molnupiravir are visually depicted in Fig. 6. A notable absorption peak in the UV spectra of CNT can be found at λmax = 477.35 nm, corresponding to an oscillator strength (f) of 0.5776. The charge transfer from the ground state (S0) to the eighth excited state (S8) is ascribed to this peak and is mainly caused by two main electron transitions: H-1 → L (51%) and H → L + 1 (46%). Furthermore, two consecutive transitions are detected, which correspond to the excited states S0 → S34 at 327.11 nm (f = 0.3819) and S0 → S33 at λmax = 327.12 nm (f = 0.3822). These transitions predominantly involve electron movements from various orbitals within the CNT structure. Upon the absorption of molnupiravir by CNT, the most intense absorption peak is due to the transition of S0 → S23 at λmax = 289 nm with an oscillator strength of 0.2725. This peak is primarily associated with charge transfer between two electron configurations, H-8 → L (38%), H-2 → L + 1 (12%), H-1 → L + 2 (−33%). Another no transition corresponds to the excited state S0 → S25 at λmax = 287 nm (f = 0.3830), primarily originating from electron transitions involving H-7 → L (41%), H-1 → L + 4 (40%) orbital. In the UV spectra of molnupiravir, prominent peaks are observed at 244 nm (f = 0.3516). Notably, these transitions are associated with weak polarization due to symmetry considerations, resulting in nearly forbidden transitions. One significant finding from our investigation is that, in contrast to the corresponding peak in isolated molnupiravir, the UV absorption peak in CNT-molnupiravir is shifted to a higher-wavelength region. This shift is referred to as a "bathochromic shift." In summary, our TDDFT calculations and UV spectra analysis provide valuable insights into the electronic transitions and absorption characteristics of CNT, molnupiravir, and their interaction.

NMR analysis

In our study, we conducted calculations and comparisons of chemical shift isotropic (CSI) and chemical shift anisotropic (CSA) values for certain particles involved in the absorption process of CNT56 and molnupiravir. We assessed how the electron density at these atoms changed due to the absorption of molnupiravir by CNT. The obtained CSI and CSA values (Table 8) were then compared with the corresponding atoms in CNT and molnupiravir molecules. Our findings shed light on the alterations in electron density. In the CNT-molnupiravir system, we observed a shift towards lower values in the CSI for carbon and hydrogen atoms in CNT, indicative of changes in electron density. Notably, the chemical shift tensors (measured in parts per million or ppm) exhibited significant alterations, especially for atoms that displayed more pronounced polarization. This suggests that atoms with greater electron density changes experienced more substantial shifts in their chemical shift tensors. Our calculations revealed a decrease in the chemical shift values after the absorption of molnupiravir by CNT, signifying increased polarization of CNT. The electron density

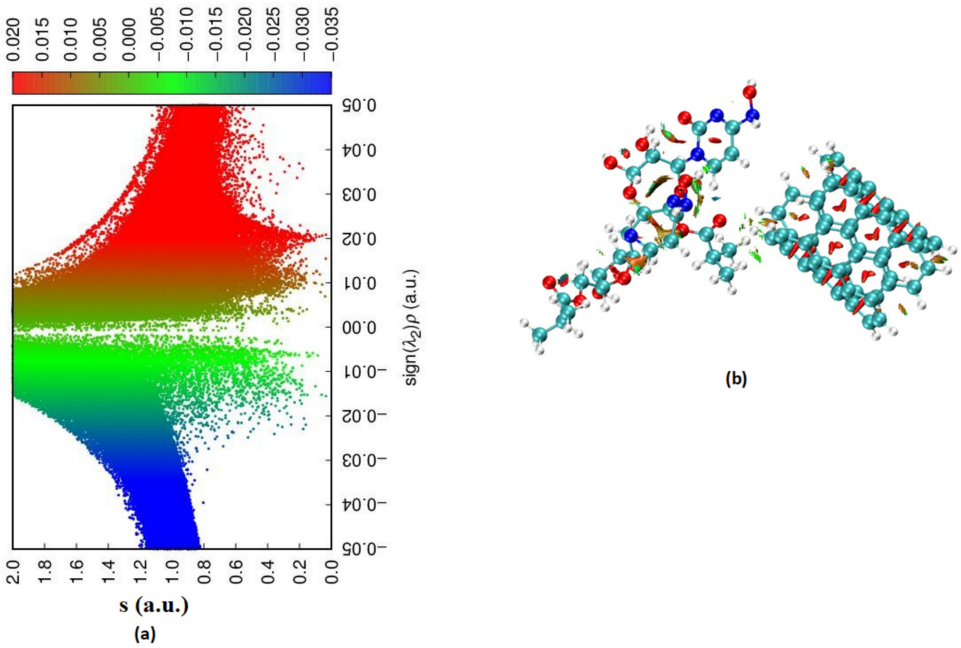


Fig. 7 **a** NON Covalent interaction analysis, **b** Orbital Overlap between CNT and MONO Density of state analysis

in the regions where molnupiravir was absorbed by CNT showed a marked increase, indicating charge transfer from one unit to another. This observation is further supported by the comparison of the theoretical IR spectra (as depicted in Supplementary Fig. 1) of CNT-molnupiravir before and after absorption. The IR peaks became more prominent post-absorption, providing additional evidence of increased polarization resulting from the interaction between CNT and molnupiravir. In summary, our study demonstrates that the absorption of molnupiravir by CNT leads to changes in electron density and polarization, which are corroborated by shifts in chemical shift tensors and more prominent IR spectra peaks in the CNT-molnupiravir system compared to the state before absorption.

NCI analysis

The non-covalent interactions within any chemical systems are explained by NCI analysis (Kumar and Mishra 1992). In essence, the reduced density gradient (s) and electron density (ρ) determine the Non-Covalent Interactions (NCI). This is dependent on the empirical finding that, at small electronic densities, non-covalent interactions can be associated with regions of minor reduced density gradient. The visualization of three-dimensional space makes use of non-covalent interactions (Thul et al. 2010).

A measure of strength causes the graphic image to rise from the reduced density gradient color's iso-surfaces. Usually, the strength is computed by multiplying the electron density at each point on the iso-surface by the second eigenvalue (λ2) of the electron density Hessian. The second eigenvalue (λ2) of the electron density Hessian determines the type of interaction. It is $\lambda 2 < 0$ for repulsive interaction and > 0 for attractive interaction. This graphic depiction has a direct bearing on the description of non-covalent interactions involving hydrogen bonds. Despite changes in molecular orbitals, NCI indexes remain constant, according to suggested electron density and derived scalar fields.

The scalar field of the electron density (ρ) is termed as reduced density gradient and calculated by using following equation

$$S_{(r)} = \frac{|\nabla \rho(r)|}{2\left(3\pi^2\right)^{\frac{1}{3}} \rho_{(r)}^{\frac{4}{3}}} \tag{13}$$

The vital modification in the abridged gradient among the intermingling atoms, in a weak inter or intra-molecular communication is present, at density critical points. The values of electron density are important parameters to determine interaction strength. In same area of density/reduced gradient both attractive and repulsive interactions are appeared. The variation of density along axis is useful to examine both repulsive and attractive interactions. The incoming net gradient flux of density ($\nabla 2\rho < 0$) or outgoing ($\nabla 2\rho > 0$) through a small volume located around a reference point is determined by the sign of the density's Laplacian ($\nabla 2\rho$). Thus, the concentration of charge density around the reference point is determined by the sign of $\nabla 2\rho$. As a result, the Laplacian's sign alone is insufficient to determine the strength of the weak interaction because the nuclei's negative contributions overcome the sign (Johnson et al. 2010).

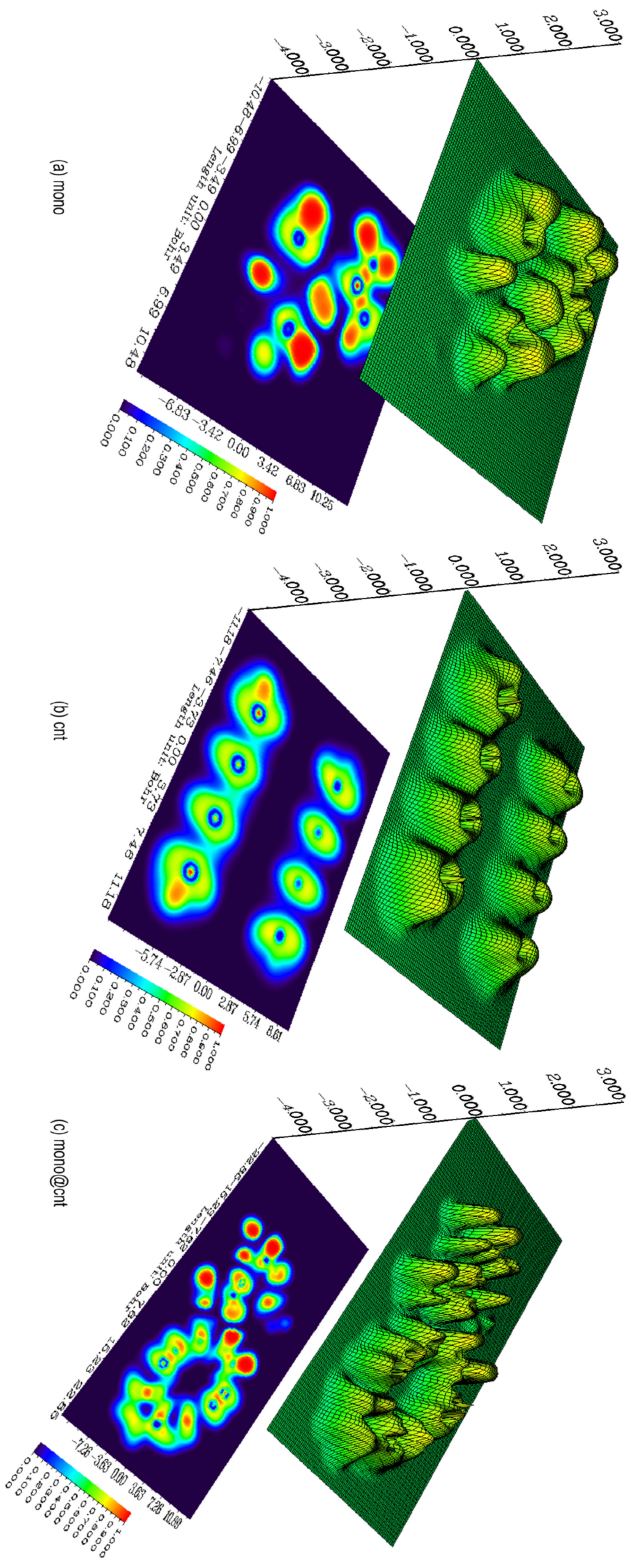


Fig. 8 ELF plot of **a** MONO, **b** CNT, **c** CNT@MONO

In this way, eigenvalue (λ_2) Laplacian electron density along the axes of interaction variation should be calculated. The sorts of exchanges are determined by symbol of second eigenvalue (λ_2). The bonding interactions, [$\lambda_2 < 0$. e.g., hydrogen bonds], are considered by a concentration of density along vertical to the bond, however Non-bonded interactions, e.g., steric repulsion $\lambda_2 > 0$arise by density reduction. The van der Waals type interactions arise due to small density overlap and for this $\lambda_2 \lesssim 0$. In this way, sign of λ_2 decides strength and nature of various types weak interactions, The graph in between abridged density gradient s(r) and sign $(\lambda_2)\rho$ is shown in Fig. 7a. The green colour 3D plots of interacting molecular orbitals of CNT@ molnupiravir which is arise due to sign$(\lambda_2)\rho$ is presented in Fig. 7a & b. The low-density, low-gradient manager for the dispersion-bound CNT with molnupiravir is lies in between 0.00 to −0.02 au show weak attraction. From this Fig. 7b weak interactions appears in between molnupiravir and CNT which is already discussed in QTAIM analysis. This aspect also shown in colour filled intermolecular surface shown in Fig. 7b.

The grey regions among the CNT and molnupiravir indicate weak Hydrogen bond type interaction respectively. These interactions are categorized with help of geometrical topological parameters. The weak interactions are comprehended among H atoms of molnupiravir drug and CNT. This weak binding has deep advantage for drug delivery that drug can easily remove from CNT and bind with targeted protein. The load exchange between molnupiravir and CNT are directly related with their orbital overlap.

Density of state analysis

The HOMO energy of MONO is 2.18 eV lower than molnupiravir -CNT complex however LUMO of CNT- molnupiravir complex is 0.94 eV higher than CNT. The lowing in energy gap indicates that excitation wave length shows red shift in CNT after absorption of molnupiravir drug. The prominent absorption peak appears at 287 nm in CNT which shows red shift of 52 nm in CNT@ molnupiravir (235 nm). The energy gap in between HOMO–LUMO of CNT@ molnupiravir complex, which is smaller than CNT, causes transfer of charges with in CNT@ molnupiravir. The Density of state shows that additional energy level inserted after same as CNT@ molnupiravir complex except additional energy level inserted in CNT molecular energy level after absorption of molnupiravir. The extra molecular energy level due to absorption of molnupiravir by CNT enhance HOMO energy level (−5.48 eV) and lowered LUMO energy level

Table 9 NBO analysis occupancy of donor (i) acceptor (j) E^2 energy of CNT@ molnupiravir

Donor NBO (*i*)	Occupancy (*i*)	Acceptor NBO (*j*)	Occupancy (*j*)	$E^{(2)}$ (kcal/mol	(*Ej–Ei*) au	*F*(*i*,*j*) au
π (C25–C26)	1.97870	σ*(N81–H113)	0.02453	1.71	0.84	0.035
π (C1–C53)	1.97890	σ*(C75–H112)	0.03750	0.78	0.87	0.024
σ (C25-–H67)	1.97672	σ*(N81–H113)	0.02453	0.58	1.10	0.022
π(C35–C44)	1.81841	σ*(N81–H113)	0.02453	0.59	0.83	0.021
Lp(1)O80	1.98324	σ*(C25–H67)	0.01578	0.70	1.26	0.027
Lp(1)O95	1.85741	σ*(C1–H70)	0.01547	0.84	1.32	0.030
Lp(2)O122	1.96786	σ*(C16–H71)	0.01682	1.25	0.95	0.031

up to (−1.53 eV) causes decrease energy gap of CNT@molnupiravir complex which is responsible for charge transfer from molnupiravir to CNT. The above discussion proves that molnupiravir drug effectively absorbed by CNT.

Electron localization function (ELF) analysis

In natural bond analysis, the electron density function is helpful in determining the electron transition from molnupiravir to CNT and from CNT to molnupiravir. Figure 8a, b, and c display the electron localization function (ELF) for molnupiravir, CNT, and CNT@ molnupiravir, respectively. While the electron density localization index value is decreasing from brown and yellow to green, the ELF values (roughly 0.8 to 1.0) are white in color. The green color lies in the middle region (0.5). The colors violet and blue are on the lower end of the scale (Program GRAPA 1989).

The ELF indicates little electron density varies after absorption of molnupiravir with CNT. The electron density of molnupiravir is changed after absorption with CNT. In CNT localization index lies in yellow region (0.70–0.80) means nearly all CNT ring is stable and electronic charge density delocalized over whole CNT. In absorption of molnupiravir by CNT ELF index of CNT and molnupiravir near interaction atoms are changes of electron density. The change in electron density of CNT after absorption of molnupiravir polarizes CNT by charge transition from molnupiravir drug. The NBO charge analysis is important tool to investigate intermolecular charge interaction. In absorption process of molnupiravir drug by CNT charge transfer from one unit to other takes place. In this process a significant contribution of 0.22 kcal/mol appears due to charge transfer from π ($C_{91}-O_{95}$) to σ*(C_1-H_{70}) which further increase to 0.27 kcal due to charge transfer to σ*(C_7-H_{72}). Another significant contribution of 0.67 kcal/mol give the impression due to charge transfer from LP (2) O_{95} to σ*(C_1-H_{70}), while further enhance up to 0.71 kcal/mol due to charge transfer to σ*(C_7-H_{72}). Clearly NBO analysis (Table 9) shows that charge transfer from MONO to CNT responsible variation of localized charge density in CNT and molnupiravir in CNT@molnupiravir complex.

Conclusion

In recent years, carbon nanotubes (CNTs) have arose as a prominent contrivance in the arena of medicine and gene delivery in biomedicine. Various methods have been projected for stacking small bio molecules, including anticancer drugs, onto nanotubes through bonded or non-bonded absorption. In this communication, we have investigated the absorption behavior of molnupiravir by CNTs using the DFT technique. The computed thermodynamic parameters reveal that the most favorable interaction corresponds to conf-1. However, it's important to note that the interaction between CNT and molnupiravir is a simultaneous exothermic reaction. Our study involved the thermodynamic optimization of the molecular geometry, which resulted in significant changes in the geometrical parameters of both molnupiravir and CNT after the absorption of molnupiravir. Notably, the energy gap of CNT increases by the absorption of molnupiravir, indicating a change in the electronic structure. Examination of the computed topological parameters at the BCP (Bond Critical Point) indicates the presence of four nonbonding interactions in the CNT-4 molnupiravir system. Moreover, our analysis of electron transfer (ECT) parameters demonstrates that electrons are transferred from molnupiravir to CNT56 during the absorption process. Furthermore, we observed significant changes in the chemical shift for interactive atoms in both CNT and molnupiravir. This study provides valuable insights and offers a novel avenue for researchers in search of innovative drug delivery systems.

Supplementary Information The online version contains supplementary material available at https://doi.org/10.1007/s43538-025-00468-1.

Acknowledgements V.S. thanks the CHPC Lengau, South Africa, for the computational facility.

Data availability Not Applicable

Declarations

Conflict of interest The authors declare that they have no conflict of interest.

References

Abdelnabi, R., Foo, C.S., Kaptein, S.J.F., Zhang, X., Do, T.N.D., Langendries, L., Vangeel, L., Breuer, J., Pang, J., Williams, R., et al.: Ebio Med **72**, 103595 (2021)

Apoorva Dwivedi, Anoop Pandey, Vijay Singh, Gaurav Mishra.: Adsorption Effects of Isoniazid Drug Over Carbon Nanotube (C56H16) and Ab-Initio Molecular Dynamics Simulation (ADMP)—A Computational Quantum Chemical Approach, October 2024, Macromolecular Symposia

Apoorva Dwivedi, Anoop Pandey, Shashwat Shukla, Vijay Singh.: A computational quantum chemical approach for surface assimilation effects of well-known voltage sensitive potassium channel blockers (4-Aminopyridine and 3,4-Diaminopyridine) over carbon nanotube, Macromolecular Symposia (2024)

Arsawang, U., Saengsawang, O., Rungrotmongkol, T., Sornmee, P., Wittayanarakul, K., Remsungnen, T., Hannongbua, S.: J. Mol. Graph. Model. **29**, 591–596 (2011)

Ayers, P.W., Parr, R.G.: J. Am. Chem. Soc. **122**(9), 2010–2018 (2000)

Bader, R.F.W.: Atoms in Molecules: A Quantum Theory (2nd edn). Oxford, New York (1990)

Bader, R.F.W.: Chem. Rev. **91**, 893–928 (1991)

Bader, F.W., Essen, H.: J. Chem. Phys. **80**, 1943 (1984)

Becke, A.D.: J ChemPhys **98**, 5648–5652 (1993a)

Becke, A.D.: J. Chem. Phys. **98**, 5648–5652 (1993b)

Bohl, M., Ponsold, K., Reck, G.: J. Steroid Biochem. **21**(4), 373–379 (1984)

Brhane, Y., Gabriel, T.: Int. J. Pharm. **7**(7), 19–27 (2016)

Celik, S.: J. Mol. Struct. **1277**, 134895 (2023)

Chen, Z., Pierre, D., He, H., Tan, S., Pham-Huy, C., Hong, H., Huang, J.: Int. J. Pharm. **28**(405), 153–161 (2011)

Cremer, D., Kraka, E.: Croat. Chem. Acta **57**, 1259–1281 (1984)

Dwivedi A., Kumar, A.: Polycyclic Aromat. Compd. (2019)

Dwivedi, A., Pandey, A.K.: Fullerenes Nanotubes Carbon Nanostruct. **22**, 679–686 (2014)

Elham Khezerloo, Y.-, Hekmat, Farzaneh, Saeed shahrokhian, Azam Irajizad.: A step toward molnupiravir, COVID-19 antiviral, detection using cauliflower-like cobalt sulfide-decorated carbon nanotube modified glassy carbon electrodes. Microchem J **204**, 111072 (2024)

Erdogdu, Y., Unsalan, O., Gulluoglu, M.T.: J. Raman Spectrosc. **41**, 820–828 (2010)

Espinosa, E., Monils, E., Lecomte, C.: Chem. Phys. Lett. **285**, 170–173 (1998)

First Oral Antiviral for COVID-19, Lagevrio (Molnupiravir), Approved by MHRA. Available online: http://www.gov.uk/government/news/first-oral-antiviral-for-covid19-lagevrio-molnupiravir-approved-by-mhra (2021)

Fleming, I.: frontier Orbitals and Organic Chemical Reactions. Wiley, New York (1976)

Frisch, A., Nelson, A. B., Holder, A. J.: GAUSSVIEW Inc., Pittsburgh PA (2000)

Frisch, M. J., Trucks, G.W., Schlegel, H. B., et.al.: Gaussian 03 Revision C.02, Gaussian Inc., Pittsburgh, PA (2003)

Geerlings, P., Proft, F.D., Langenaeker, W.: Chem. Rev. **103**, 1793–1874 (2003)

Heister, E., Neves, V., Lamprecht, C., Silva, S., Coley, H., McFadden, J.: Carbon **50**, 622–632 (2012)

Jiménez-Alberto, A., Ribas-Aparicio, R.M., Aparicio-Ozores, G., Castelán-Vega, J.A.: Comput. Biol. Chem. **88**, 107325 (2020)

Johnson, E.R., Keinan, S., Mori-Sanchez, P., Contreras- Garcia, J., Cohen, A.J., Yang, W.: J. Am. Chem. Soc. **132**, 6498–6506 (2010)

Koch, U., Popelier, P.: J. Phys. Chem., A **99**, 9747 (1995)

Kumar, A., Mishra, P.C.: J. Mol. Struct. **277**, 299–312 (1992)

Lamberti, M., Pedata, P., Sannolo, N., Porto, S., De Rosa, A., Caraglia, M.: Int. J. Immunopathol. Pharmacol. **28**(1), 4–13 (2015)

Lee, C., Yang, W., Parr, R.G.: Phys. Rev. B **37**, 785–789 (1988)

Lewis, D.F., Griffiths, V.: Informa Healthcare **17**, 769–776 (1987)

Lijima, S.: Nature **354**(6348), 56–58 (1991)

Liu, Z., Sun, X., Nakayama-Ratchford, N., Dai, H.: ACS Nano **1**(1), 50–59 (2007a)

Liu, Z., Winters, M., Holodniy, M., Dai, H.: Angew. Chem. Int. Ed. Engl. **46**, 2023–2027 (2007b)

Liu, Z., Cai, W., He, L., Nakayama, N., Chen, K., Sun, X., Chen, X., Dai, H.: Nat. Nanotechnol. **2**, 47–52 (2007c)

Matta, I. F., Boyd, R. J.: Wiley-VCH Verlag Gmbh (2007)

Misra, N., Dwivedi, A., Pandey, A.: Chin. J. Phys. **50**(1), 64–75 (2012)

Murray, J.S., Sen, K.: Molecular Electrostatic Potential, Concepts and Applications. Elsevier, Amsterdam (1996)

O'Boyle, N.M., Tenderholt, A.L., Langner, K.M.: J. Comp. Chem. **29**, 839–845 (2008)

Padmanabhan, J., Parthasarathi, R., Subramaniaan, V., Chattaraj, P.K.: J. Phys. Chem. A **111**, 1358–1361 (2007)

Parr, R.G., Pearson, R.G.: J. Am. Chem. Soc. **105**, 7512–7516 (1983)

Parr, R.G., Szentpály, L., Liu, S.: J. Am. Chem. Soc. **121**, 1922–1924 (1999)

Program GRAPA: J. Flad, E-X. Fraschio, B. Miehlich, Institut fur Theoreti sche Chemie der Universitat, Stuttgart (1989)

Rozas, I., Alkorta, I., Elguero, J.: Behavior of Ylides Containing N, O, and C Atoms as Hydrogen Bond Acceptors. J. Am. Chem. Soc. **122**(45), 11154–11161 (2000)

Thul, P., Gupta, V.P., Ram, V.J., Tandon, P.: Spectrochim. Acta **7**, 251–260 (2010)

Tiwari, G., Sharma, D., Singh, N.B.: J Sci Ind Res (India) **79**, 337 (2020)

Tiwari, G., Chauhan, M.S., Sharma, D.: Polycycl. Aromat. Compd. **43**, 1 (2022a)

Tiwari, G., Chauhan, M.S., Sharma, D.: Polycycl. Aromat. Compd. **42**, 7256 (2022b)

X-Yahya, S., Alqahtania, Ashraf M. Mahmouda, Mohamed M. El-Wekil, Hossieny Ibrahim.: Surface engineering of carbon microspheres with nanoceria wrapped on MWCNTs: a dual electrocatalyst for simultaneous monitoring of molnupiravir and paracetamol. RSC Adv. **14**, 5406–5416 (2024)

Publisher's Note Springer Nature remains neutral with regard to jurisdictional claims in published maps and institutional affiliations.

Springer Nature or its licensor (e.g. a society or other partner) holds exclusive rights to this article under a publishing agreement with the author(s) or other rightsholder(s); author self-archiving of the accepted manuscript version of this article is solely governed by the terms of such publishing agreement and applicable law.